

Effects of post-sinter annealing on microstructure and magnetic properties of Nd-Fe-B sintered magnets with Nd-Ga intergranular addition

Jin-Hao Zhu(朱金豪), Lei Jin(金磊), Zhe-Huan Jin(金哲欢), Guang-Fei Ding(丁广飞), Bo Zheng(郑波), Shuai Guo(郭帅), Ren-Jie Chen(陈仁杰), and A-Ru Yan(闫阿儒)

Citation: Chin. Phys. B, 2021, 30 (**6**): 067503. DOI: 10.1088/1674-1056/abddad
Journal homepage: http://cpb.iphy.ac.cn; http://iopscience.iop.org/cpb

What follows is a list of articles you may be interested in

Coercivity and microstructure of sintered Nd-Fe-B magnets diffused with Pr-Co, Pr-Al, and Pr-Co-Al alloys

Lei Jin(金磊), Zhe-Huan Jin(金哲欢), Jin-Hao Zhu(朱金豪), Guang-Fei Ding(丁广飞), Bo Zheng(郑波) , Shuai Guo(郭帅), Ren-Jie Chen(陈仁杰), A-Ru Yan(闫阿儒), and Xin-Cai Liu(刘新才)

Chin. Phys. B, 2021, 30 (**2**): 027503. DOI: 10.1088/1674-1056/abc166

Effect of annealing temperature on coercivity of Nd-Fe-B magnets with TbFeAl doping by process of hot-pressing

Ze-Teng Shu(舒泽腾), Bo Zheng(郑波), Guang-Fei Ding(丁广飞), Shi-Cong Liao(廖是聪), Jing-Hui Di(邸敬慧), Shuai Guo(郭帅), Ren-Jie Chen(陈仁杰), A-Ru Yan(闫阿儒), Lei Shi(石磊)

Chin. Phys. B, 2020, 29 (**5**): 057501. DOI: 10.1088/1674-1056/ab7b57

Grain boundary restructuring and La/Ce/Y application in Nd-Fe-B magnets

Mi Yan(严密), Jiaying Jin(金佳莹), Tianyu Ma(马天宇)

Chin. Phys. B, 2019, 28 (**7**): 077507. DOI: 10.1088/1674-1056/28/7/077507

Magnetic properties of misch-metal partially substituted Nd-Fe-B magnets sintered by dual alloy method

Jie-Fu Xiong(熊杰夫), Rong-Xiang Shang(商荣翔), Yan-Li Liu(刘艳丽), Xin Zhao(赵鑫), Wen-Liang Zuo(左文亮), Feng-Xia Hu(胡凤霞), Ji-Rong Sun(孙继荣), Tong-Yun Zhao(赵同云), Ren-Jie Chen(陈仁杰), Bao-Gen Shen(沈保根)

Chin. Phys. B, 2018, 27 (**7**): 077504. DOI: 10.1088/1674-1056/27/7/077504

Effects of terbium sulfide addition on magnetic properties, microstructure and thermal stability of sintered Nd—Fe—B magnets

Xiang-Bin Li(李向斌), Shuo Liu(刘硕), Xue-Jing Cao(曹学静), Bei-Bei Zhou(周贝贝), Ling Chen(陈岭), A-Ru Yan(闫阿儒), Gao-Lin Yan(严高林)

Chin. Phys. B, 2016, 25 (**7**): 077502. DOI: 10.1088/1674-1056/25/7/077502

Effects of post-sinter annealing on microstructure and magnetic properties of Nd–Fe–B sintered magnets with Nd–Ga intergranular addition*

Jin-Hao Zhu(朱金豪)[1,2], Lei Jin(金磊)[1], Zhe-Huan Jin(金哲欢)[1], Guang-Fei Ding(丁广飞)[1,†], Bo Zheng(郑波)[1], Shuai Guo(郭帅)[1,2,‡], Ren-Jie Chen(陈仁杰)[1,2], and A-Ru Yan(闫阿儒)[1,2]

[1] *CAS Key Laboratory of Magnetic Materials and Devices, and Zhejiang Province Key Laboratory of Magnetic Materials and Application Technology, Ningbo Institute of Materials Technology and Engineering, Chinese Academy of Sciences (CAS), Ningbo* 315201, *China*

[2] *University of Chinese Academy of Sciences, Beijing* 100049, *China*

(Received 7 December 2020; revised manuscript received 15 January 2021; accepted manuscript online 20 January 2021)

We investigate the effects of post-sinter annealing on the microstructure and magnetic properties in B-lean Nd–Fe–B sintered magnets with different quantities of Nd–Ga intergranular additions. The magnet with fewer Nd–Ga additions can enhance 0.2 T in coercivity, with its remanences nearly unchanged after annealing. With the further increase of the Nd–Ga addition, the annealing process leads coercivity to increase 0.4 T, accompanied by a slight decrease of remanence. With the Nd–Ga addition further increasing and after annealing, however, the increase of coercivity is basically constant and the change of remanence is reduced. Microstructure observation indicates that the matrix grains are covered by continuous thin grain boundary phase in the magnets with an appropriate Nd–Ga concentration after the annealing process. However, the exceeding Nd–Ga addition brings out notable segregation of grain boundary phase, and prior formation of part $RE_6Fe_{13}Ga$ phase in the sintered magnet. This prior formation results in a weaker change of remanence after the annealing process. Therefore, the diverse changes of magnetic properties with different Nd–Ga concentrations are based on the respective evolution of grain boundary after the annealing process.

Keywords: Nd–Fe–B magnet, magnetic properties, grain boundary, microstructures

PACS: 75.60.Nt, 75.50.Ww, 75.50.Vv, 75.60.Ej **DOI:** 10.1088/1674-1056/abddad

1. Introduction

The 2:14:1-type Nd–Fe–B magnets with excellent magnetic performance have been widely used in traction motors of electric vehicles, wind turbines and other fields.[1–3] As heavy rare-earth (HRE) resources are limited and expensive, it is urgent to find other effective ways of avoiding the abuse of expensive elements to stabilize the performance of the magnets at high temperature operation. Based on the nucleation fields theory,[4,5] the achievement of high coercivity relies on the modification in the averaged local effective demagnetization factor and microstructural parameter for the Nd–Fe–B sintered magnets without HRE. Grain refinement has been an effective approach to improve the coercivity by reducing the demagnetization effect of the grains,[6–9] but it is also limited by process cost and equipment conditions.

On the other hand, the annealing process is a significant way to improve the microstructures in grain boundary (GB) areas. It is generally accepted that the thin GB phase is formed mainly by the infiltration of liquid from the triple junction phase (TJP) during the annealing process. And the morphology of the GB phase/main grain interface becomes smooth after the annealing process.[10,11] In order to strengthen the effect of the annealing process and improve the wettability of the GB phase, metal elements formed low melting points alloy with rare-earths (RE), such as Cu, Ga, and Al, were discussed.[12–14] In addition, the distribution of these trace alloy elements was influenced by the annealing process, especially Cu atoms were enriched in the Nd-rich/$Nd_2Fe_{14}B$ interface after the annealing process.[15,16] By adjusting the distribution and composition of the GB phase, the RE-M (M = Al, Cu) is reported to be beneficial for high coercivity through addition or grain boundary diffusion process after annealing process.[17–20]

Recently, the Nd–Fe–B magnets prepared from Nd-rich Ga-doped Nd–Fe–B strip cast flakes have become an important object of research.[21,22] In these Ga-doped magnets, continuous GB phases were formed which brings out the isolated intergrain exchange coupling. Note that unlike the conventional magnets, these significant changes in microstructure and coercivity of Ga-doped magnets are accompanied by the formation of anti-ferromagnetic $RE_6Fe_{13}Ga$ (RE = Pr, Nd) phase after the annealing process. This GB phase formation process is affected by grain boundary composition,[23,24] and the

*Project supported by the Major Project of Science and Technology Innovation 2025 in Ningbo, China (Grant No. 2018B10086) , the Major Project of Inner Mongolia Science and Technology, Zhejiang Provincial Public Welfare Technology Application Research Project, China (Grant No. LGG21E010007), and the Key Research and Development Program of Shandong Province, China (Grant No. 2019JZZY010321).

†Corresponding author. E-mail: dingguangfei@nimte.ac.cn

‡Corresponding author. E-mail: gshuai@nimte.ac.cn

© 2021 Chinese Physical Society and IOP Publishing Ltd

preparation conditions as well.[25,26]

In this work, we investigate the microstructures and magnetic properties of B-lean Nd–Fe–B sintered and annealed magnets with different quantities of Nd–Ga additions. According to the sensitive dependence of the formation of the $RE_6Fe_{13}Ga$ phase on the composition and the annealing process, the effects of the annealing process on the magnets with different compositions of the GB phase are systematically investigated based on the characterization, microstructure and elemental distributions of phase constituents.

2. Experiment

In this experiment, the master alloy with the nominal compositions of $(PrNd)_{32}Fe_{bal.}(CuAlCoZr)_{1.75}B_{0.88}$ (wt% in content ratio) were prepared by strip casting. These strips were subjected to the hydrogen decrepitated process and the jet milling process to obtain the Nd–Fe–B powders (~ 2.8 μm in size). Then, the $Nd_{77.5}Ga_{22.5}$ (wt% in content ratio) powders (~ 2.5 μm in size) were also obtained by the similar process. The Nd–Fe–B powders mixed with different content ratios of the Nd–Ga powders (0, 1, 2, 3, 4, 8 wt%) were compacted with a magnetic field 1800 kA/m followed by isostatic pressing at 150 MPa. Afterwards, the sintering process was performed at 1030 °C–1040 °C for 2 h in vacuum, followed by argon gas quenching, accordingly obtaining the as-sintered magnets (AS). The as-sintered samples were also annealed at 500 °C for 2 h in vacuum, accordingly obtaining the annealed magnets (AN). Hereafter, the Nd–Fe–B magnets with different Nd–Ga concentrations were named 0NG–8NG samples.

Magnetic properties of sintered and annealed magnets were measured by pulsed field magnetometer (PFM) (HIRST PFM14.CN) at a temperature of 20 °C. The constitution of phase was identified by x-ray diffraction (XRD) (Bruker D8 Advance Davinci) using Cu $K\alpha$ radiation. The microstructures and element distribution of the magnets were observed by using the back scatter electron scanning electron microscopy (BSE-SEM) equipped with energy dispersive x-ray spectroscopy (EDS) detector, and the scanning/transmission electron microscope (S/TEM) (Talos F200X) with energy dispersive x-ray spectroscopy (EDS) signal detection.

3. Results and discussion

Figures 1(a) and 1(b) show the diverse effects of the annealing process on the magnetic properties in magnets with different Nd–Ga additions. In the annealed magnets with fewer Nd–Ga additions as shown in area I, the remanence (B_r) is unchanged basically and the coercivity (H_{cj}) is increased slightly compared with in the sintered magnets. It is similar to the effect of the annealing process on the conventional magnet. With the further increase of Nd–Ga addition shown in area II, the B_r of the annealed magnet has a slight decrease relative to that of the sintered magnets, while the change of H_{cj} continues to increase after the annealing process. Finally, with the excessive addition of Nd–Ga shown in area III, the increase in H_{cj} of the magnet remains basically unchanged after annealing, while the change in B_r becomes smaller. Thus, the annealed magnet with 4-wt% Nd–Ga addition is considered to have excellent comprehensive magnetic properties. Table 1 shows the magnetic properties of representative samples from the areas I, II, and III.

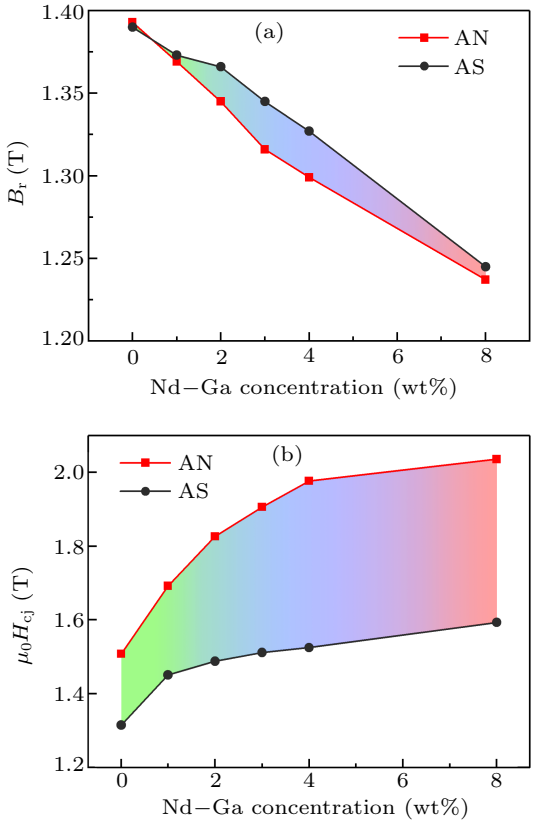


Fig. 1. Diverse effects of annealing process on (a) remanence and (b) coercivity in magnets with Nd–Ga concentrations.

Table 1. Values of remanence B_r, coercivity $\mu_0 H_{cj}$, and maximum energy product $(BH)_{max}$ of samples.

Sample	B_r (T)	$\mu_0 H_c$ (T)	$(BH)_{max}$ (kJ/m^3)
0NG-AS	1.39	1.31	367
0NG-AN	1.39	1.51	375
4NG-AS	1.33	1.53	339
4NG-AN	1.30	1.98	325
8NG-AS	1.25	1.59	302
8NG-AN	1.24	2.04	290

In order to investigate the effects of the annealing process on the phase composition of anisotropic magnets with 0%, 4%, and 8% (wt%) Nd–Ga concentration, XRD analyses are performed as shown in Fig. 2. The tested plane is perpendicular to the C axis. Neither the annealing process nor the addition of Nd–Ga is found to have a significant effect on the grain orientation in the anisotropic magnets, where their ratios of relative intensity, $I_{(006)}/I_{(105)}$, range about from 0.95 to 1.00.

The characteristic peaks of the $Nd_6Fe_{13}Ga$ phase are detected in the 4NG sample after being annealed, and compared with in the 0NG. The diffraction peaks of the $Nd_6Fe_{13}Ga$ phase slightly shift toward the low-angle region. It is considered that Pr atoms are substituted for part of Nd atoms at the $RE_6Fe_{13}Ga$ phase, in which the radius of Pr atom in the alloy is larger than that of Nd atom due to lanthanide contraction. In addition, the characteristic peaks of $Nd_6Fe_{13}Ga$ are also detected in the 8NG-AN sample, which corresponds strictly to its standard peak. Therefore, the introduction of Ga by intergranular addition of Nd–Ga is similar to alloy melting. It results in the formation of $Nd_6Fe_{13}Ga$ phase regulated by the appropriate composition and annealing process. What is worth noting is that the characteristic peaks of the $Nd_6Fe_{13}Ga$ are measured in the 8NG-AS sample similarly. Thus the excess Nd–Ga addition leads the $Nd_6Fe_{13}Ga$ phase to form in sintered magnet.

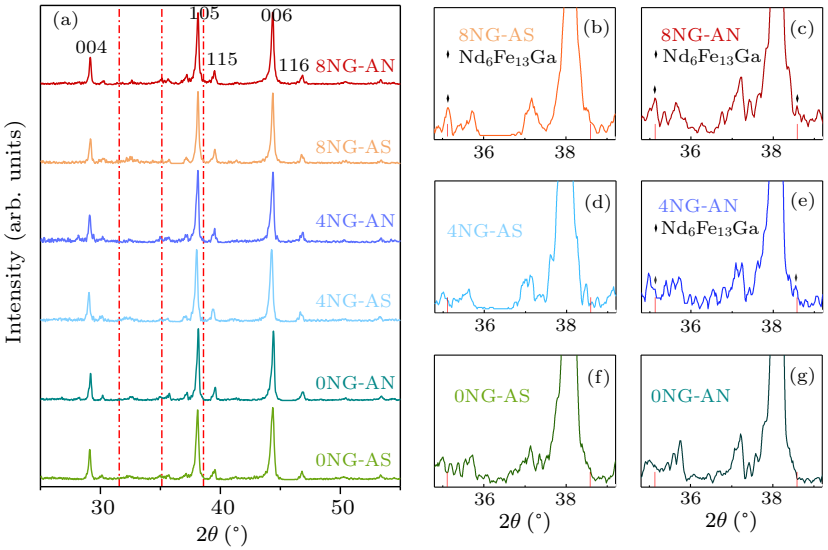


Fig. 2. (a) XRD profiles of the anisotropic as-sintered and annealed magnets with 0%, 4%, and 8% (wt%) Nd–Ga concentration, with tested plane being perpendicular to *C* axis. [(b)–(g)] XRD partial enlarged view of the corresponding samples, with red perpendicular line indicating three strongest peaks of $Nd_6Fe_{13}Ga$ in XRD.

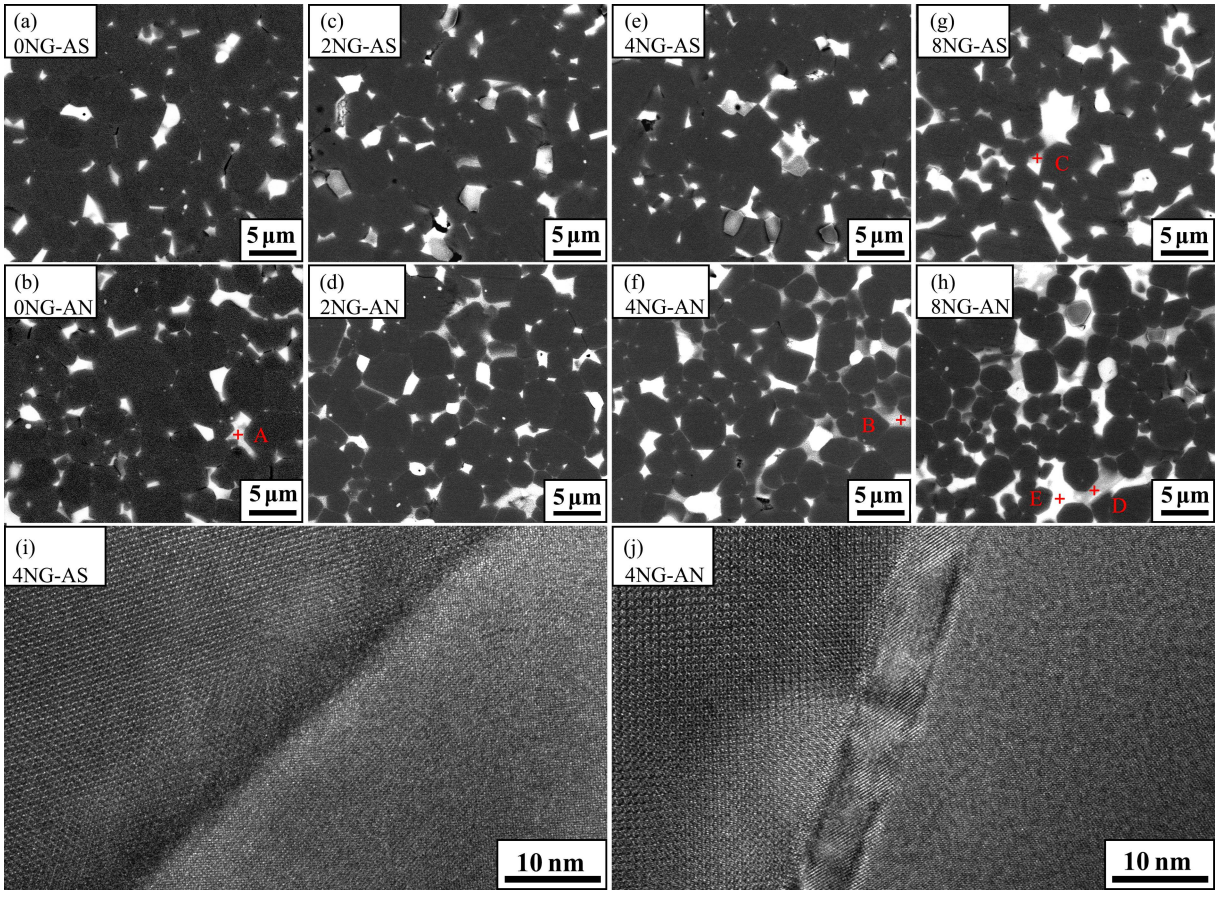


Fig. 3. BSE SEM images of as-sintered and annealed magnets with Nd–Ga concentration of [(a)–(h)] 0%–8% (wt%). HRTEM images of GB phases of (e) as-sintered and (d) annealed magnets with Nd–Ga concentration of 4% (wt%). Observed plane is perpendicular to *C* axis.

Figures 3(a)–3(h) show backscattered electron (BSE) SEM images taken from the as-sintered and annealed magnets with Nd–Ga concentration in a range of of 0%–8% (wt%). The observed plane is perpendicular to the *C* axis. In the original B-lean magnet without Nd–Ga addition, Fe and Cu are enriched in the TJP according to the EDS quantitative analysis shown in Table 2. This enrichment of Fe in the GB area is beneficial to the subsequent addition of Nd–Ga to induce the $Nd_6Fe_{13}Ga$ phase to form. With the Nd–Ga addition increasing, the proportion of TJP in the sintered magnet is enhanced. Besides, the continuous thin GB phase forms in the annealed magnet with Nd–Ga addition, and some GB phases with dim contrast are confirmed to be RE_6Fe_{13}(Ga, Cu) phase by further EDS quantitative analysis in Table 2, such as points B and D. Moreover, a small number of $Nd_6Fe_{12}(Ga, Cu)_2$ phases are found at the edge of the TJP in the 8NG-AS sample, and the excessive Nd–Ga phases are observed in the triple junctions in the 8NG-AN sample. It indicates that under the excess Nd–Ga addition, $RE_6(Fe, Ga)_{14}$ phase trends to form in the cooling process, with residual Nd–Ga phase remaining in TJP. The high-resolution (HR) TEM bright field images of interface between adjacent grains in 4NG-AS and 4NG-AN samples are shown in Figs. 3(i) and 3(j). Comparing with in the sintered sample, a continuous thin GB phase is generated after the annealing process has contributed to the intergrain exchange decoupling.

Table 2. EDS analysis results of selected areas in Fig. 3.

Position	Element (at.%)			
	Pr+Nd	Fe	Ga	Cu
A	23.2	65.3	/	2.40
B	33.1	58.4	4.63	0.39
C	29.9	57.5	8.66	0.79
D	27.9	57.9	4.90	0.25
E	69.2	7.36	20.1	1.81

To further investigate the prior formation of GB phase in sintered magnets with excess Nd–Ga addition, TEM characterizations are carried out to obtain the detailed microstructure and element distribution features. The observed plane is perpendicular to the *C* axis. Figure 4 shows the bright field TEM images and HAADF-STEM images of the 8NG-AS sample, where the TJP is surrounded by matrix grains. Further, there are observed two different GB phases in the GB area in sintered samples. Through EDS elemental maps and spectra obtained from points A and B, the detailed results of EDS are summarized in Table 3, there is the $RE_6Fe_{13}Ga$ phase found at the edge of part matrix phases marked in dark green, and the GB phase marked in light green is considered to be the Nd(Ga, Cu) phase. Therefore, in the cooling process after sintering, the $RE_6Fe_{13}Ga$ phase formation occurs partially at TJP along the edge of the part matrix phase with the excessive addition of Nd–Ga. The results of TEM characterizations correspond with the XRD and SEM analysis. Thus, a part of antiferromagnetic $RE_6Fe_{13}Ga$ phases formed by RE, Ga, and Cu reacting with ferromagnetic element regulate the magnetism of part of GB phases in sintered magnets ahead of time.

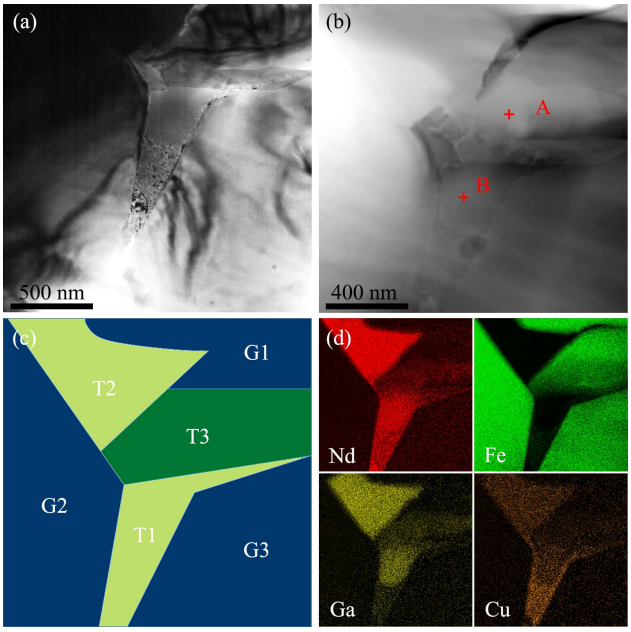


Fig. 4. (a) Bright field TEM image, (b) HAADF-STEM image, (c) corresponding schematic image, and (d) EDS elemental maps of triple junction in the 8NG as-sintered sample. Matrix grains are marked in dark blue and GB phases are marked in light green and dark green in the corresponding schematic image. Observed plane is perpendicular to *C* axis.

Table 3. Detailed results of EDS in Fig. 4(b), with O element decreasing.

Position	Element (at.%)			
	Pr+Nd	Fe	Ga	Cu
A	23.5	66.7	6.37	1.46
B	62.3	5.65	25.4	5.39

Figure 5 schematically illustrates the respective evolution of the grain boundary structure in sintered magnets with different Nd–Ga additions after annealing. For the magnet with fewer Nd–Ga additions, the composition and distribution of the GB phase have not been optimized, thus the change in the magnetic properties of the magnet is similar to that of the conventional magnet after it has been annealed. With the appropriate Nd–Ga addition in B-lean magnet, the $RE_6Fe_{13}Ga$ phase and continuous GB phase are generated after it has been annealed. This formation of the GB phase by the annealing process results in a significant enhancement of the H_{cj} value, while the further increase of Nd–Ga addition can only dilute the matrix grain proportion and form a part of $RE_6Fe_{13}Ga$ phases in the sintered magnet. The analyses of microstructure and magnetic properties indicate that after the annealing process, the formation of the non-ferromagnetic $RE_6Fe_{13}Ga$ phase triggers the formation of continuous GB phase, leading the B_r value to slightly decrease, while the continuous thin GB

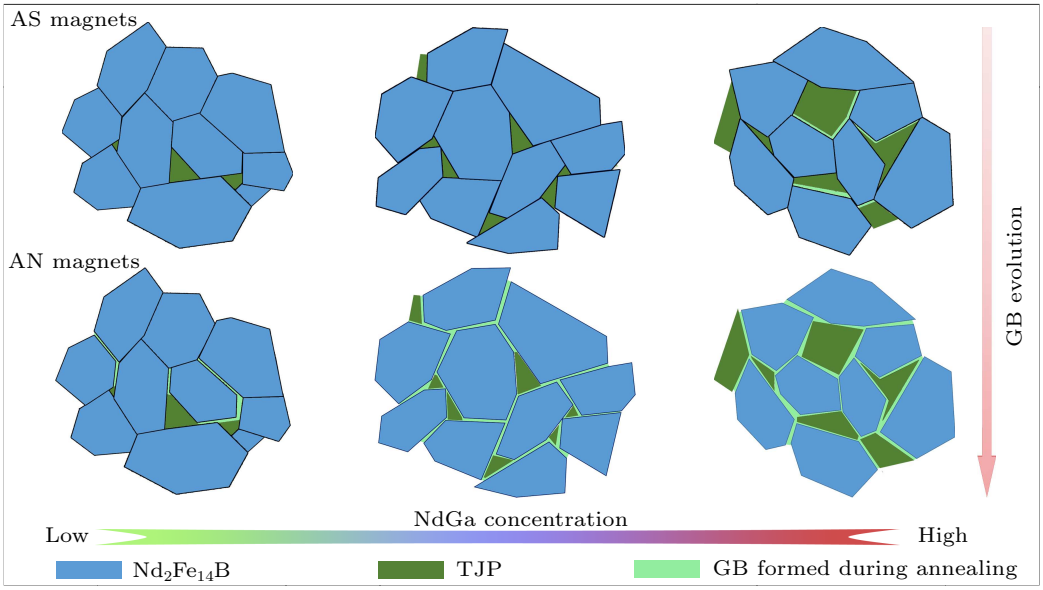


Fig. 5. Schematic illustrations of respective evolution of grain boundaries of magnets with different Nd–Ga additions after annealing.

phase isolating the matrix grain is the major factor of the significant improvement in H_{cj} rather than the formation of the $RE_6Fe_{13}Ga$ phase itself at TJP. Therefore, the excess addition of Nd–Ga in magnets cannot strengthen the effect of the annealing process in enhancing H_{cj}, and prior formation of the GB phase at triple junctions leads to a weaker change in B_r after the annealing process.

4. Conclusions

In this work, the effects of the annealing process on the microstructure and magnetic properties of the B-lean Nd–Fe–B magnets with different Nd–Ga additions are investigated systematically. The characterization of phase constituents and microstructure reflect that the appropriate Nd–Ga concentration in magnets after being annealed can bring out the continuous thin GB phase and formation of the non-ferromagnetic $RE_6Fe_{13}Ga$ phase. This GB composition and annealing process can optimize the microstructure effectively to facilitate the intergrain exchange decoupling, resulting in a significant improvement of H_{cj} accompanied with a slight decrease of B_r after the annealing process. However, the excessive Nd–Ga addition cannot further optimize the microstructure, resulting in a limited H_{cj} increment. In addition, a part of $RE_6Fe_{13}Ga$ phases are found at TJP along the edge of a part of matrix phases in sintered magnet with excessive addition, giving rise to a weaker change in B_r after the annealing process. Therefore, the respective evolution of grain boundary after the annealing process leads to the diverse change of magnetic properties in magnets with different Nd–Ga additions.

References

[1] Sagawa M, Fujimura S, Togawa N, Yamamoto H and Matsuura Y 1984 *J. Appl. Phys.* **55** 2083
[2] Sugimoto S 2011 *J. Phys. D: Appl. Phys.* **44** 064001
[3] Nakamura H 2018 *Scr. Mater.* **154** 273
[4] Kronmuller H, Durst K and Sagawa M 1988 *J. Magn. Magn. Mater.* **74** 291
[5] Kronmuller H 1987 *Phys. Status Solidi B* **144** 385
[6] Scott D, Ma B M, Liang Y L and Bounds C 1996 *J. Appl. Phys.* **79** 5501
[7] Bance S, Seebacher B, Schrefl T, Exl L, Winklhofer M, Hrkac G, Zimanyi G, Shoji T, Yano M, Sakuma N, Ito M, Kato A and Manabe A 2014 *J. Appl. Phys.* **116** 233903
[8] Sepehri-Amin H, Ohkubo Y, Gruber M, Schrefl T and Hono K 2014 *Scr. Mater.* **89** 29
[9] Ding G F, Guo S, Chen L, Di J H, Chen K, Chen R J, Lee D and Yan A R 2018 *J. Alloys Compd.* **735** 1176
[10] Vial F, Joly F, Nevalainen E, Sagawa M, Hiraga K and Park K 2002 *J. Magn. Magn. Mater.* **242** 1329
[11] Park D, Kim T, Lee S, Kim D and Jang T 2010 *J. Appl. Phys.* **107** 09a737
[12] Chen F G, Jin Y X, Cheng Y and Zhang L T 2018 *Scr. Mater.* **157** 135
[13] Knoch K, Grieb B, Henig E, Kronmuller H and Petzow G 1990 *IEEE Trans. Magn.* **26** 1951
[14] Goto R, Nishio S, Matsuura M, Tezuka N and Sugimoto S 2008 *IEEE Trans. Magn.* **44** 4232
[15] Li W, Ohkubo T and Hono K 2009 *Acta Mater.* **57** 1337
[16] Yang Y Q, Si H G, Yang H, Zhang L, Huang D F, Chen B Y, Chen B Y, Xu F, Hu Y M and Han B J 2018 *Phys. Lett. A* **382** 135
[17] Zeng H X, Liu Z W, Li W, Zhang J S, Zhao L Z, Zhong X C, Yu H Y and Guo B C 2019 *J. Magn. Magn. Mater.* **471** 97
[18] Shu Z T, Zheng B, Ding G F, Liao S C, Di J H, Guo S, Chen R J, Yan A R and Shi L 2020 *Chin. Phys. B* **29** 057501
[19] Jin L, Jin Z H, Zhu J H, Ding G F, Zheng B, Guo S, Chen R J, Yan A R and Liu X C 2021 *Chin. Phys. B* **30** 027503
[20] Lu K C, Bao X Q, Chen G X, Zhang X J, Tang M H, Mu X, Li J H and Gao X X 2019 *Scr. Mater.* **160** 86
[21] Sasaki T, Ohkubo T, Takada Y, Sato T, Kato A, Kaneko Y and Hono K 2016 *Scr. Mater.* **113** 218
[22] Enokido Y, Miwa M, Goto S and Fujikawa Y 2016 *Mater. Trans.* **57** 1960
[23] Grieb B, Pithan C, Henig E and Petzow G 1991 *J. Appl. Phys.* **70** 6354
[24] Xu X D, Dong Z J, Sasaki T, Tang X, Sepehri-Amin H, Ohkubo T and Hono K 2019 *J. Alloys Compd.* **806** 1267
[25] Sasaki T, Takada Y, Okazaki H, Ohkubo T, Nakamura T, Sato T, Kato A, Kaneko Y and Hono K 2019 *J. Alloys Compd.* **790** 750
[26] Ding G F, Guo S, Chen L, Di J H, Song J, Chen R J, Lee D and Yan A R 2018 *J. Alloys Compd.* **735** 795